



HAL
open science

A simple 1-D radiative-convective atmospheric model designed for integration into coupled models of magma ocean planets

Emmanuel Marcq

► **To cite this version:**

Emmanuel Marcq. A simple 1-D radiative-convective atmospheric model designed for integration into coupled models of magma ocean planets. *Journal of Geophysical Research. Planets*, 2012, 117 (E1), pp.E01001. 10.1029/2011JE003912. hal-00639286

HAL Id: hal-00639286

<https://hal.science/hal-00639286>

Submitted on 11 Feb 2016

HAL is a multi-disciplinary open access archive for the deposit and dissemination of scientific research documents, whether they are published or not. The documents may come from teaching and research institutions in France or abroad, or from public or private research centers.

L'archive ouverte pluridisciplinaire **HAL**, est destinée au dépôt et à la diffusion de documents scientifiques de niveau recherche, publiés ou non, émanant des établissements d'enseignement et de recherche français ou étrangers, des laboratoires publics ou privés.

A simple 1-D radiative-convective atmospheric model designed for integration into coupled models of magma ocean planets

E. Marcq¹

Received 29 July 2011; revised 31 October 2011; accepted 1 November 2011; published 5 January 2012.

[1] In order to understand the early history of telluric interiors and atmospheres during the ocean magma stage, a coupled interior-atmosphere-escape model is being developed. This paper describes the atmospheric part and its first preliminary results. A unidimensional, radiative-convective, H₂O-CO₂ atmosphere is modeled following a vertical $T(z)$ profile similar to Kasting (1988) and Abe and Matsui (1988). Opacities in the thermal IR are then computed using a k -correlated code (KSPECTRUM), tabulated continuum opacities for H₂O-H₂O and CO₂-CO₂ absorption, and water or sulphuric acid clouds in the moist convective zone (whenever present). The first results show the existence of two regimes depending on the relative value of the surface temperature T_s compared to a threshold temperature T_c depending on the total gaseous inventory. For $T_s < T_c$, efficient blanketing results in a cool upper atmosphere, a cloud cover, and a long lifetime for the underneath magma ocean with a net thermal IR flux between 160 and 200 Wm⁻². For $T_s > T_c$, the blanketing is not efficient enough to prevent large radiative heat loss to space through a hot, cloudless atmosphere. Our current calculations may underestimate the thermal flux in the case of hot surfaces with little gaseous content in the atmosphere.

Citation: Marcq, E. (2012), A simple 1-D radiative-convective atmospheric model designed for integration into coupled models of magma ocean planets, *J. Geophys. Res.*, 117, E01001, doi:10.1029/2011JE003912.

1. Introduction

[2] Understanding the early history of telluric planets is a topic of paramount importance for two reasons: first, in order to investigate the reasons that set Earth and Venus, and to a lesser extent Mars, on very different evolutionary paths and, second, because understanding which range of initial conditions (planet size, stellar flux, volatile inventory, etc.) ultimately results in a telluric atmosphere similar to ours, to Venus', or to some other kind not found in the solar system is highly needed since we are on the verge of characterizing such planets in our galactic neighborhood. A relatively short stage of the evolution of telluric planets is called the magma ocean stage: short-lived isotopes and accretion heat cause temperatures high enough for the mantle to be in a liquid state, with little to no solid crust. At the same time, a secondary atmosphere (N₂-CO₂-H₂O, for example) is present, more or less effectively insulating the planet from radiative heat loss. The atmospheric content during this stage is also leaking to interplanetary space due to escape processes (collisional, impact-related, etc.). Understanding the planetary evolution during this stage therefore requires coupled models in order to get a sensible understanding.

[3] Some coupled models already exist, but they usually feature very simplistic atmospheres [Elkins-Tanton, 2008;

Abe, 1997], usually parameterized by a single parameter, their IR optical depth. On the other hand, more realistic atmospheric models exist for similar atmospheres such as Earth's future atmosphere after a H₂O runaway greenhouse [Kasting, 1988] or before the condensation of water oceans [Abe and Matsui, 1988]. But these models were not coupled to interior models. Kasting's model was, however, subsequently coupled with an accretion model and an atmospheric escape model [Zahnle *et al.*, 1988].

[4] Consequently, a team led by É. Chassefière (IDES, Orsay, France) and involving H. Massol and T. Lebrun (IDES, Orsay, France) for the interior modeling, E. Marcq (LATMOS, Guyancourt, France) for the atmospheric model, and F. Leblanc (LATMOS, Paris, France) for modeling atmospheric escape has begun working on such a coupled model. This paper deals with the first part of the model that has reached an operational stage, namely, the atmospheric model. Other papers describing the relevant parts of the model should follow shortly (as of 2011).

2. Description of the Model

[5] Our computer model, written in Fortran 90, is unidimensional, extending from the surface up to an altitude of 600 km. It takes into account convective and radiative processes in the atmosphere. The gas mixture is assumed to consist solely of water vapor as a condensable species, and carbon dioxide as a noncondensable species. Future inclusion of gaseous nitrogen is possible but assuming typical volatile inventories in the early history of terrestrial planets, it should amount to a few percents of total pressure at most and thus its

¹LATMOS, Université de Versailles Saint-Quentin-en-Yvelines, Guyancourt, France.

inclusion would not alter the results significantly. The only situation where inclusion of N_2 would be necessary is whether the temperature profile causes CO_2 to condense also, leaving N_2 as a ultimate noncondensable species in the upper atmosphere.

[6] Recent studies [Hashimoto *et al.*, 2007; Schaefer and Fegley, 2010] have pointed out the possibility of a reducing atmosphere at this stage. The most abundant species would then be H_2 , CH_4 , and/or CO , with a variable water vapor content. Nevertheless, qualitative results of this study should not depend too much on the exact atmospheric composition provided H_2O is abundant enough (minimal partial surface pressure at least 10^6 Pa): as will be shown in section 3.1, H_2O dominates most of the outgoing thermal IR spectrum. Reducing species would then play a role similar to CO_2 in the present study, acting as noncondensable species with some IR opacity.

[7] Please note that we always consider CO_2 as an ideal gas, but H_2O vapor obeys a more complicated equation of state computed from NBS/NRC steam tables embedded in Fortran [Haar *et al.*, 1984]. It enables the model to remain valid even close to the liquid-vapor equilibrium in the water phase diagram. Validity close to the critical point of water vapor ($P_c = 22.06$ MPa, $T_c = 647.1$ K) is not guaranteed, however [Kasting, 1988; Ingersoll, 1969; Abe and Matsui, 1988]. This is not much of a concern: in a realistic atmosphere, the (P,T) profile would not approach this critical point according to Kasting [1988]. Following the convention of Kasting [1988], all physical variables indexed by v deal with water vapor, and those indexed by n deal with CO_2 .

2.1. Integration Into Coupled Models

[8] As previously stated, this atmospheric model is designed for integration into coupled models. As such, it needs other components of the coupled model for inputs, and provides outputs for them.

2.1.1. Inputs

[9] The interactive inputs are (1) surface temperature T_s , assumed to be equal the temperature of the lowest atmospheric layer since, as on present-day Venus, the solid surface is not expected to be directly heated by solar radiation and (2) surface pressures of gaseous species, namely, water vapor P_v and carbon dioxide P_n . Other, noninteractive input are also required, such as the solar constant. They will be discussed separately wherever relevant in the paper.

2.1.2. Outputs

[10] Anything the model computes can be considered to be an output, but usually other parts would need, more specifically, (1) net radiative flux escaping into space F_{net} and (2) upper boundary (mesopause) conditions: mesopause temperature T_0 and density and mixing ratios of H_2O and CO_2 at mesopause level. The net radiative flux is especially critical since it constrains the cooling time of the magma ocean. The outgoing thermal flux F is usually expressed in terms of effective temperature T_{eff} such as: $F = \sigma T_{eff}^4$ with σ standing for the Stefan-Boltzmann constant. Since magma ocean planets are still cooling, they are not in radiative equilibrium if we consider long time scales, and as such this effective temperature is greater than the equilibrium temperature T_{eq} defined by: $\sigma T_{eq}^4 = (1 - A)C$ where C stands for the averaged solar constant ($C = 239 \text{ Wm}^{-2}$ at 1UA assuming a 70% luminosity for the early Sun) and A the bolometric

albedo integrated for solar wavelengths. We then have $F_{net} = \sigma(T_{eff}^4 - T_{eq}^4)$.

2.2. Computation of Vertical Structure

[11] The atmosphere is assumed be plane parallel since its maximal scale height is by far smaller than the planetary radius. It is discretized into eight hundred 750 m thick computational layers. Following Kasting [1988], we group these layers in a three physical layer structure from the top of the atmosphere down below: (1) an isothermal mesosphere in approximate radiative equilibrium, (2) optionally, a moist troposphere where the partial pressure of water vapor P_v is equal to its saturation value, and (3) a dry troposphere where $P_v < P_{sat}(T)$ or where $T > T_c$, the critical temperature for water vapor.

[12] If the moist troposphere extends down to the surface, then we expect the formation of a water ocean, bringing an effective end to the magma ocean stage. Dry atmospheres will exhibit only two physical layers: dry troposphere with an overlying mesosphere. Let us detail the description of these physical layers.

2.2.1. Dry Troposphere

[13] If the surface vapor pressure of water vapor does not exceed the saturation value, a dry troposphere exists. Since heat transfer is dominated by convective processes in this layer, the thermal gradient is expected to follow a (dry) adiabat $\Gamma_d = (dT/dz)_S$. Furthermore, the mixing ratio of water vapor density relative to CO_2 , $\alpha_v = \rho_v/\rho_n$, does not vary with altitude in this mixed layer where no condensation occurs. The following expression for Γ_d is adapted from Appendix A of Kasting [1988]:

$$\Gamma_d = -g \frac{\rho_n + \left[T \left(\frac{\partial V}{\partial T} \right)_P \right]^{-1}}{\rho_n C_{p,n}(T) + \left[T \left(\frac{\partial V}{\partial T} \right)_P \right]^{-1} C_{p,v}(T)},$$

where V stands for the specific volume.

[14] This expression yields the usual expression $\Gamma_d = -g/C_p$ in the case of a pure H_2O or a pure CO_2 atmosphere. $C_{p,v}(T)$ is provided by the steam tables, and we use for $C_{p,n}(T)$ the polynomial expression from Abe and Matsui [1988].

[15] Once Γ_d is known, dP_n/dz can be computed using the fact that $d\alpha_v/dz = 0$. dP_v/dz is then computed assuming hydrostatic equilibrium, and densities ρ_v and ρ_n are then computed from the relevant equations of state for the overlying computational layer, integrating vertical profiles upward.

2.2.2. Moist Troposphere

[16] In the moist layer, condensation of H_2O takes place, yielding $d\alpha_v/dz < 0$. We then substitute the equation $P_v = P_{sat}(T)$ instead, and according to Appendix A of Kasting [1988], we have

$$\Gamma_m = \frac{-\rho g}{\frac{dP_{sat}}{dT} + R\rho_n/M_n \left(1 + \frac{d \ln \rho_n}{d \ln T} - \frac{d \ln \alpha_v}{d \ln T} \right)},$$

where M_n stands for the molecular weight of CO_2 ,

$$\frac{d \ln \alpha_v}{d \ln T} = \frac{R/M_n (d \ln \rho_v / d \ln T) - C_{v,n}(T) - \alpha_v (ds_v / d \ln T)}{\alpha_v [s_v - s_c] + R/M_n},$$

and s_c stands for the specific entropy of (condensed) liquid water, also computed from the steam tables. We then simply have $dP_v/dz = \Gamma_m(dP_{\text{sat}}/dT)$, and dP_n/dz is found assuming hydrostatic equilibrium.

[17] The top of the moist layer is reached, where $T(z)$ falls below the mesospheric temperature T_0 that is discussed in section 2.2.3.

2.2.3. Mesosphere

[18] *Kasting* [1988] assumed that the purely radiative layer (mesosphere) was isothermal with $T_0 = 200$ K. Actually, it could be possible to compute a realistic $T(z)$ profile so that we cancel out the divergence of the radiative heat flux computed in part in this layer. However, because of computation time constraints caused by the embedding in a complex model, we opted for a minor yet significant improvement.

[19] Following ideas expressed by *Taylor* [2006], T_0 is now set at the skin temperature in the gray, two-stream approximation: $T_0 = 2^{-1/4}T_{\text{eff}}$. Since T_{eff} depends on T_0 , some iterations (usually less than five) are needed so that the temperature profile becomes radiatively self-consistent at the top of the atmosphere. As expected, we could check a posteriori that the divergence of radiative heat flux for vanishing thermal IR opacity is very small; our criterion to halt iterative adjustment of T_0 is $|d\ln F/d\tau| < 0.02$. Of course, full radiative equilibrium may not be reached for T_0 because shortwave opacity is not taken into account properly (our model would be unable to reproduce Earth's stratosphere, for example), so that we proceeded to sensitivity studies with prescribed values of T_0 in section 3.2.1. *Kasting* [1988] investigated the effect of altering T_0 from 200 K to 250 K and concluded that there was no change in T_{eff} for this range of T_0 , but the atmospheres we investigate may differ quite dramatically from the runaway H₂O greenhouse that was the focus of *Kasting* [1988].

[20] Please also note that α_v is constant in this mixed layer since no condensation takes place. Of course, if a moist troposphere lies below, α_v in the mesosphere will be lower than α_v in the dry troposphere; water vapor is caught in a “cold trap” in such a case.

2.3. Computation of Radiative Balance

[21] Since the atmospheric layers able to radiate to space are found to be cooler than 700 K, we could legitimately separate radiative fluxes between longwave (thermal) and shortwave (solar). The longwave domain extends from 0 to 10,000 cm⁻¹ (1 μm).

[22] Shortwave radiation is computed in a fast, but very crude way, parameterized only by the equilibrium temperature T_{eq} defined in section 2.1.2. The fact that the temperature profile is prescribed rather than computed from radiative fluxes makes this parameterization legitimate. This also implies that the mesosphere is assumed to be perfectly transparent in shortwave radiation. This is equivalent to say that we are dismissing the possible existence of a stratosphere (defined as a nonconvective atmospheric layer where $dT/dz > 0$), which is legitimate since both H₂O and CO₂ are very effective thermal radiators.

[23] Longwave radiation is treated in 36 separate spectral interval (bands), in which opacities are computed using a k -correlated code for line opacities and tabulated continuum opacities. The radiative equations are then solved using

DISORT [*Stammes et al.*, 1988] in a two-stream approximation. Absorption and scattering by cloud particles is also included. Since $\lambda > 1 \mu\text{m}$, Rayleigh scattering was not taken into account.

[24] Details about the computation of longwave opacities are described in sections 2.3.1–2.3.3.

2.3.1. Line Opacities

[25] Opacity caused by the absorption lines of H₂O and CO₂ were computed in two stages. First of all, the Fortran program KSPECTRUM designed by V. Eymet was used to compute high-resolution spectra (with fully resolved absorption lines and line truncation at 100 cm⁻¹ since far wing opacities are normally computed as part of the continuum; see section 2.3.2) for temperature ranging from 200 up to 750 K, total pressure ranging from 1 Pa up to 10⁶ Pa and mixing ratio of H₂O relative to CO₂ ranging from 10⁻⁹ up to 1–10⁻⁴. Please note that KSPECTRUM has already been used in previous studies of H₂O-CO₂ atmospheres, mainly for Mars and terrestrial exoplanetary atmospheres [*Wordsworth et al.*, 2010, 2011]. Also, although higher pressures and temperatures are sometimes encountered in the deeper layers of the atmosphere, they lie deep enough so that they are usually unable to radiate through space and so it is unimportant to compute precisely opacities for such deep computational layers.

[26] Then, according to the usual k -correlated method, each of these spectra was processed in each of the 36 discrete bands to yield only 16 $k(g)$ absorption coefficients for the 16 g values according to the statistical distribution function of absorption coefficients. Multilinear interpolation in $\{T, \log P, \log(P_v/P_n)\}$ is then performed to obtain the 16 $k(g)$ coefficients in each computational layer with a column density of gaseous molecules n . opacity can then be computed using:

$$\tau = -\ln \left[\int_0^1 e^{-k(g)n} dg \right] \approx -\ln \left[\sum_{i=1}^{16} e^{-k(g_i)n} \Delta g_i \right].$$

[27] Former similar studies such as those by *Kasting* [1988] and *Abe and Matsui* [1988] computed opacities using a random band model instead, but they are known to overestimate opacities (and therefore underestimate thermal emission), in particular where scattering takes place. Because of the decrease in computation cost since the late 1980s, we could afford switching from a random band model to a k -correlated model at the cost of roughly one week of computation time on the Institut Pierre Simon Laplace (IPSL) computer cluster for the high-resolution spectra.

2.3.2. Continuum Opacities

[28] In the densest layers, we have to take into account collision induced absorption (CIA). CO₂-CO₂ CIA parameters from 200 to 750 K were read in look-up tables obtained from Bézard's Venus thermal radiation model [*Bézard et al.*, 1990]. We will show later than brightness temperature of the outgoing thermal radiation never exceeds this value, so there is no need to know the CO₂-CO₂ CIA at higher temperatures.

[29] H₂O-H₂O CIA was read from look-up tables obtained after running the MT-CKD computer program [*Clough et al.*, 2005] between 200 and 700 K. H₂O-CO₂ CIA is not yet taken into account, since it was found to be completely dominated by H₂O-H₂O continuum in the denser, warmer and water vapor-rich layers.

Table 1. IR Optical Properties of Clouds

	Earth-Like Clouds	Venus-Like Clouds
Relative mass loading	4×10^{-4}	10^{-5}
Extinction coefficient at $1 \mu\text{m}$ (m^2kg^{-1})	130	400
ϖ_0	1, $\lambda < 1 \mu\text{m}$ $1.24\lambda^{-0.32}$, $\lambda > 1 \mu\text{m}$	1, $\lambda < 2.21 \mu\text{m}$ $e^{1.16-1.42\log\lambda-0.05\log^2\lambda}$, $\lambda > 2.21 \mu\text{m}$
g	0.85, $\lambda < 10 \mu\text{m}$ $1.4\lambda^{-0.22}$, $\lambda > 10 \mu\text{m}$	0.73, $\lambda < 3.37 \mu\text{m}$ $7.28\lambda^{-1.89}$, $\lambda > 3.37 \mu\text{m}$
Q_{ext}	1, $\lambda < 20 \mu\text{m}$ $3.26\lambda^{-0.32}$, $\lambda > 20 \mu\text{m}$	1, $\lambda < 5.63 \mu\text{m}$ $10.86\lambda^{-1.38}$, $\lambda > 5.63 \mu\text{m}$

2.3.3. Clouds

[30] Cloud opacity and scattering in the longwave domain is also taken into account. The optical properties are either identical to *Kasting* [1988], therefore assuming a simplified Mie behavior of liquid water cloud droplets with a mean $5 \mu\text{m}$ radius or Venus-like, assuming a simplified Mie behavior of 75%–25% $\text{H}_2\text{SO}_4\text{-H}_2\text{O}$ with a mean radius of $1.1 \mu\text{m}$.

[31] Here $\varpi_0(\lambda)$, $g(\lambda)$, and $Q_{\text{ext}}(\lambda)$ are given in both cases by analytical approximations detailed in Table 1. Earth-like clouds are expected considering the expected availability of water in $\text{H}_2\text{O-CO}_2$ atmospheres, but inclusion of the Venus-like case is of interest for two main reasons. First, it is possible that sulphur-bearing gases exist and are abundant enough (and water partial pressure low enough at higher altitudes) to contaminate water droplets, so that acidic clouds are an actual possibility in such atmospheres. Second, these clouds are the only optically thick clouds known to exist on another telluric planet, and the fact that they are very different from Earth's expands the scope of our model. However, unless mentioned otherwise, our study assumes Earth-like clouds since they are the most likely type of clouds encountered in steam atmospheres.

[32] The cloud layers are assumed to extend throughout the whole moist convective zone. Mass loading proportional to the gaseous density is also considered as done by *Kasting* [1988], with a minor difference: a smoother transition between the clear layers (mesosphere and dry troposphere) and the cloud region is performed in the lowest and highest scale height of the moist convective zone. This situation, reminiscent of Venus, enables a smooth transition during the cooling of the atmosphere of a magma ocean planet from a cloud-free regime to a fully overcast regime.

[33] The effect of the clouds on the shortwave bolometric albedo A is only roughly parameterized, according to the simple formula: $A = [1 - \exp(-\tau_c)]A_c + \exp(-\tau_c)A_0$, where τ_c stands for the vertical, integrated cloud opacity at $1 \mu\text{m}$, A_0 the albedo in the cloud-free regime and A_c the albedo of the clouds themselves. Reasonable values for A_0 and A_c have been prescribed as $A_0 = 0.2$, and $A_c = 0.7$ according to the value for present-day Venus.

3. Results

[34] Even though this model is intended to be used as a part of coupled magma ocean/atmosphere models, there are nevertheless a few stand-alone experiments that can be performed to establish its validity and give some physical insight: (1) on the possible evolution of these atmospheres, especially on the possibility of having a water ocean

formation and (2) on the detectability of exoplanets currently in this stage using their thermal infrared radiation.

3.1. Early Earth in Magma Ocean Stage

3.1.1. T_{eff} versus T_{surf}

[35] As can be seen in Figure 1, there are two distinct regimes where T_s falls above or below a threshold temperature T_c . Assuming an Earth-like volatile inventory ($P_v = 300$ bars and $P_n = 100$ bars), we have $T_c \approx 2350$ K. T_c is an increasing function of both P_v and P_n .

[36] In the $T_s < T_c$ this regime, T_{eff} does not depend on T_s within less than 1 K. Its relatively low value (less than 250 K) is indicative of what *Elkins-Tanton* [2008] and *Abe and Matsui* [1988] called a blanketing effect, akin to the greenhouse effect. In this regime, the atmosphere is very thick and comparatively not hot enough so that the layers able to radiate to space are similar to those of planets in long-term radiative equilibrium (for which $T_{\text{eff}} \sim T_{\text{eq}}$). The relatively high albedo (low T_{eq}) in this regime also indicates that cloud layers exist in the moist convective region. Although there are striking differences (abundance of water vapor especially), the atmosphere in this case is quite reminiscent of Venus with a dry troposphere extending for several scale heights before encountering the cloud layers and finally a comparatively cool mesosphere.

[37] In the $T_s > T_c$ regime, the blanketing effect described above is not as efficient. Temperatures are too hot, so that even the radiative layers are significantly warmer than they would be if the planet were in radiative equilibrium. A rapid cooling would ensue, bringing the planet in the blanketing regime after a geologically brief time interval (up to 10^5 years

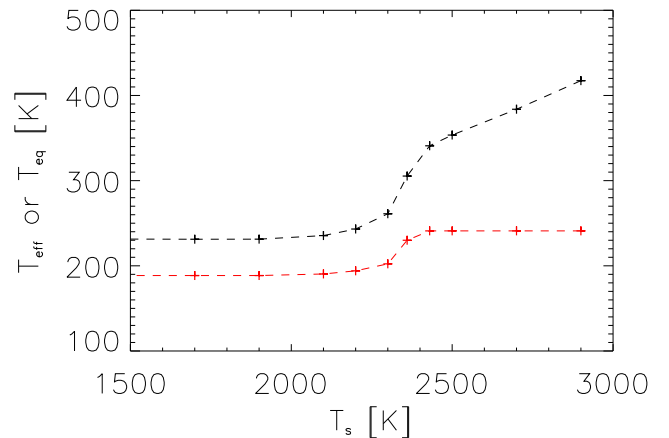


Figure 1. T_{eff} (black line) and T_{eq} (red line) versus T_s with $P_n = 100$ bars and $P_v = 300$ bars.

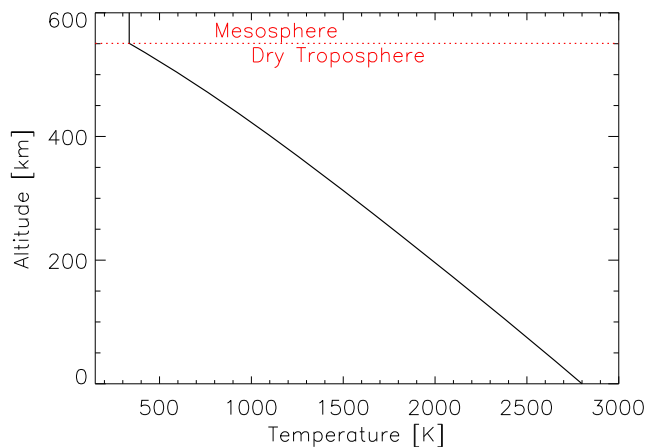


Figure 2. $T(z)$ profile with $T_s = 2800$ K, $P_n = 100$ bars, and $P_v = 300$ bars.

according to preliminary tests of a coupled model). Note also that in this regime, temperatures are too hot in the whole vertical extent of this atmosphere, preventing condensation of water vapor (relatively low albedo). Such atmospheres have no analog in the present-day solar system.

[38] We shall now investigate more in detail two specific modeled atmospheres pertaining to these two regimes.

3.1.2. $T_s > T_c$

[39] The temperature profile assuming $T_s = 2800$ K is shown in Figure 2. As previously stated, a dry troposphere lies directly below the warm mesosphere ($T_0 = 335$ K), with no moist troposphere and therefore no cloud layer. The spectrum of the outgoing thermal radiation is shown in Figure 3. The strong opacity of a H_2O - CO_2 mixture is particularly striking here: brightness temperatures never exceed 650 K, which is the actual temperature at an altitude of about 500 km. Furthermore, brightness temperature is greater than T_{eff} only in a few narrow windows shortward of $4 \mu\text{m}$, where continua opacities are significantly less than at longer wavelengths. Once again, the situation here is quite similar to the case of Venus, where brightness temperature is quite low except in a few so-called “infrared windows”. In this case, the windows are even narrower because of H_2O opacity, which plays only a minor role on Venus [Meadows and Crisp, 1996]. Also, it is worth noting that out of the bands, $T_B \simeq T_0$ and since the mesosphere is isothermal, absorption features of H_2O and CO_2 are not as prominent as could be expected.

[40] The detection of exoplanets in such a stage of their evolution could be nevertheless be possible in the thermal infrared range, since the relatively high effective temperature ($T_{\text{eff}} = 398$ K in this simulation) would yield a spectral radiance ratio between the Sun and such a planet on the order of 100 at $\lambda = 12 \mu\text{m}$.

[41] Finally, we note that there is no cold trap at all in this atmosphere: α_v remains constant with altitude from top to bottom. This means that efficient escape of water is possible during this stage, but more quantitative conclusions can only be stated in the frame of a coupled model including escape processes.

3.1.3. $T_s < T_c$

[42] The temperature profile assuming $T_s = 1400$ K is shown in Figure 4. This time, a 100 km thick moist

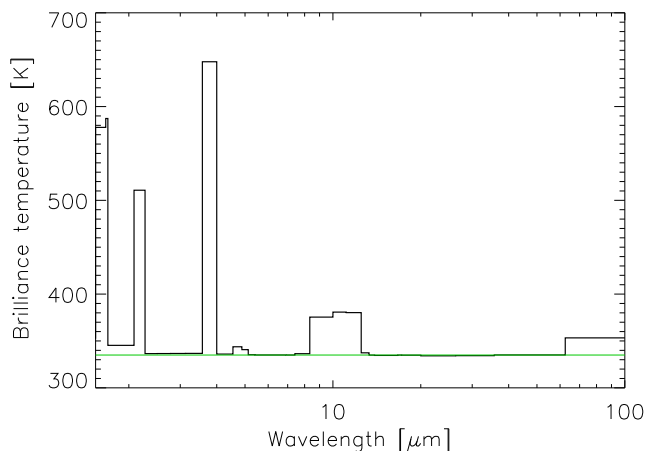


Figure 3. Brightness temperature T_B of thermal emission for the same atmosphere as in Figure 2. The green line stands for actual mesospheric temperature $T_B = T_0$.

convective layer can be seen ranging from 200 km up to 300 km, and water condensation is expected in this zone. Mesospheric temperature is this time close to 195 K, demonstrating an efficient blanketing effect. The spectrum of the outgoing thermal radiation is shown in Figure 5. In this case, thermal radiation originates mostly from the moist convective layer ($T_B < 280$ K) but not below because of the cloud scattering; the infrared windows discussed in section 3.1.2 still exist, but their brightness temperature has dramatically decreased. H_2O (especially between 6 and 7 μm) and CO_2 (especially near 15 μm) bands are visible in absorption, which is expected since $dT/dz < 0$ in the moist convective region. H_2O dominates most of the spectrum, except near 15 μm .

[43] Detectability of exoplanets in this stage of their evolution appears more challenging, since their brightness temperature is always moderate. Furthermore, provided they could be detected, it may be hard to make a distinction between this class of magma ocean planets and more evolved, solid surface planets with CO_2 - H_2O atmospheres in radiative equilibrium. Incidentally, this latter type of

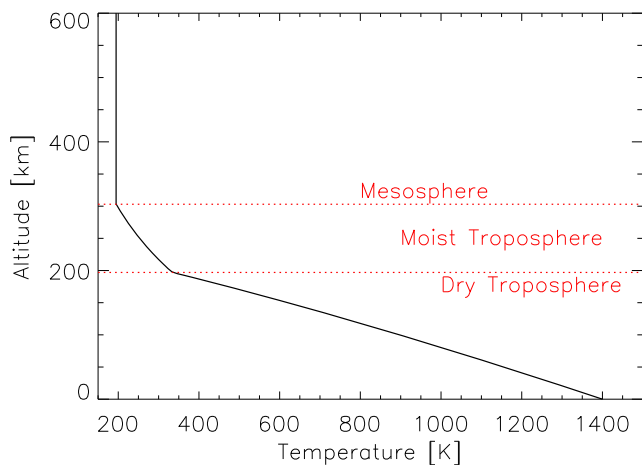


Figure 4. $T(z)$ profile with $T_s = 1400$ K, $P_n = 100$ bars, and $P_v = 300$ bars.

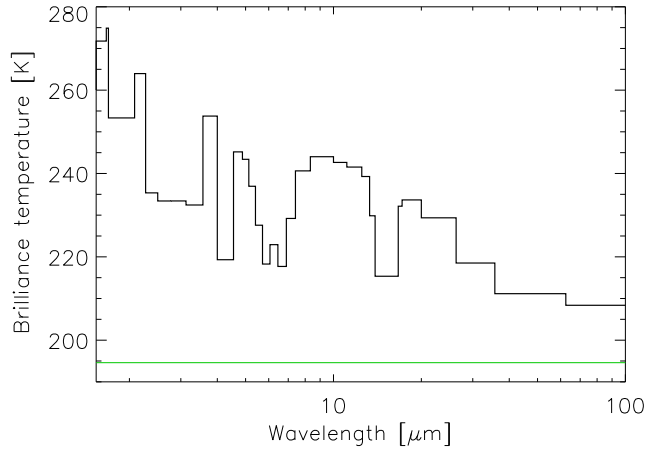


Figure 5. Brightness temperature T_B of thermal emission for the same atmosphere as in Figure 4. The green line stands for actual mesospheric temperature $T_B = T_0$.

atmosphere is a privileged target of astrobiology for they exhibit CO_2 and H_2O signatures. O_3 signature may be useful to make a distinction then, since little O_2 (and therefore O_3) is expected during the magma ocean stage.

[44] Although T_c is a function of the volatile inventory as shown in Table 2, T_{eff} in this case is quite constant for atmospheres dominated by water vapor opacity, yielding an outgoing infrared flux between 160 W m^{-2} and 170 W m^{-2} depending on the relative abundance of CO_2 . This limit is known in runaway greenhouse studies as the Komabayashi-Ingersoll (KI) limit [Nakajima *et al.*, 1992; Komabayashi, 1967; Ingersoll, 1969]. Our value is about twice less than previous models' estimates. Nevertheless, our estimate is, as far as we know, the only computation of this limit for a nongray atmosphere, so their value was probably overestimated; other preliminary studies working on the same topic report also lower values for the KI limit (J. F. Kasting, private communication, 2011).

[45] This low KI limit raises an interesting question since it is actually lower than the 240 W m^{-2} emitted by present-day Earth. Of course, some results and/or assumptions of our model do not apply to present-day Earth: higher surface pressures, optically thick atmospheres, no water ocean. Thus, our results merely suggest that, were a $\text{H}_2\text{O-CO}_2$ runaway greenhouse reached on Earth, it could sustain a radiative equilibrium with solar input. But our model is unable to model the transition between present-day conditions on Earth and a runaway greenhouse, so that the stability domains of

Table 2. T_c and Asymptotic F Versus P_n and P_v ^a

P_v (bars)	P_n (bars)	F (W m^{-2})	T_c (K)
300	100	162.9	2350
100	30	163.7	1980
30	10	163.5	1625
10	3	164.4	1380
100	0.3	172	2150
30	0.1	172.2	1750
300	300	160	2200
10	10	160	1250

^aEarth-like clouds are assumed.

present-day conditions and runaway greenhouse conditions may overlap, which would imply that atmospheric stability is subject to some level of hysteresis, much akin to the overlapping stability domain of present-day conditions and snowball Earth conditions. Furthermore, the possible dependency of the KI limit with optical cloud properties (see section 3.2.2) prevents us from determining precisely any tipping point to a runaway greenhouse state starting from present-day conditions.

3.2. Sensitivity Studies

3.2.1. Mesospheric Temperature

[46] As mentioned earlier, the mesospheric temperature T_0 may not be in IR radiative equilibrium since it might have a relatively strong opacity at solar wavelengths, enabling it to be directly heated by the Sun. Investigations with a prescribed T_0 (and thus a mesosphere out of radiative equilibrium in the longwave domain) are shown in Figure 6. Variations of T_{eff} for all cloud scenarios are negligible for $T_0 < 220 \text{ K}$, but not for greater values. This can be understood as the mesosphere gets much wetter at higher temperatures, thereby increasing dramatically its longwave opacity and thus its contribution to the net thermal emission. It also highlights that hotter mesospheres are required for $T_s > T_c$ in order to enable efficient radiative cooling of the atmosphere. For $T_s < T_c$, we think that $T_0 > 220 \text{ K}$ is unrealistic for two main reasons. First, since IR opacity of the mesosphere increases dramatically with increasing T_0 , the required shortwave opacity to maintain radiative balance is very high in a $\text{H}_2\text{O-CO}_2$ atmosphere. Actually, in CO_2 dominated atmospheres such as Mars' or Venus', no stratospheric temperature inversion is possible. Second, an isothermal and optically thick mesosphere are mutually exclusive: IR radiative equilibrium in the whole vertical extent of the mesosphere would create a negative dT/dz gradient. For our model to be self-consistent, mesospheric temperatures have to be relatively low compared to the effective temperature, and our heuristic mentioned in section 2.2.3 is a natural way to achieve this.

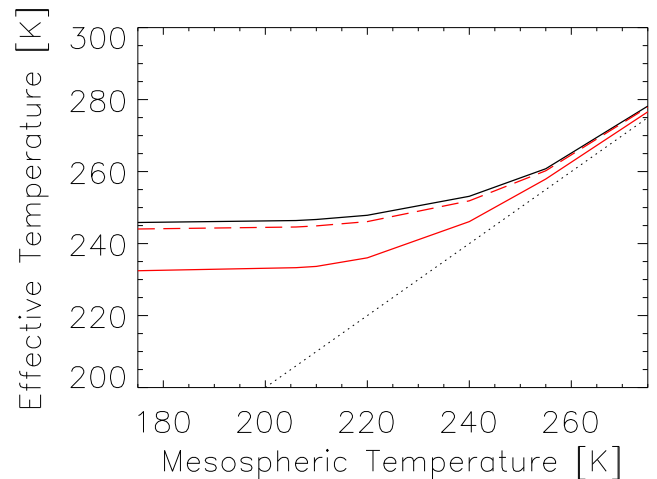


Figure 6. Effective temperature versus T_0 . Solid black line stands for the cloudless case, dashed red line is for Venus-like clouds, and solid red line is for Earth-like clouds. The dotted line is $T_{\text{eff}} = T_0$.

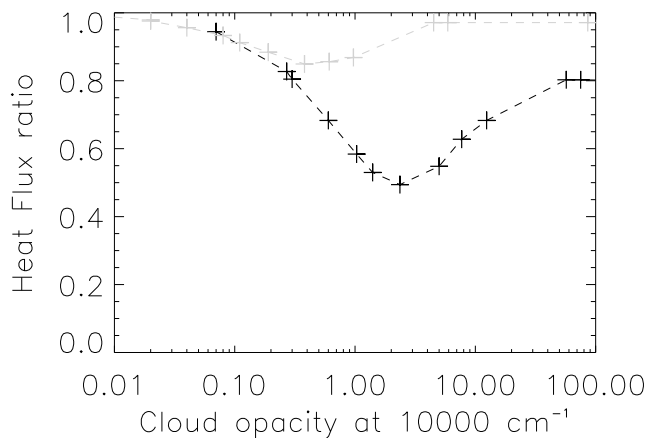


Figure 7. Ratio of outgoing thermal flux for Venus-like clouds (gray line) and Earth-like clouds (black line) upon thermal flux in a cloudless case.

3.2.2. Clouds

[47] Since optical depth of the clouds is not directly set in our studies, a possible way to investigate the radiative effect of clouds is to alter total pressure and surface temperature so that cloud layer form at diverse pressure layers, thereby with varying optical depth. Results are shown in Figure 7. The behavior at lower cloud opacities is straightforward since optically thin cloud layer are not expected to impact radiative budget. Also expectedly, the effect of clouds is to decrease the thermal emission through nonconservative scattering by cloud particles, and the effect is peaking when cloud opacity lies in the interval $\tau_c = 10^{-1} \sim 10$. However, there are several differences with previous studies of their effect such as the one by *Kasting* [1988]. First, the maximal effect reported here is much bigger, ranging from a moderate decrease of 15% for small sulphuric acid droplets up to a 50% decrease for Earth-like clouds. And second, whereas *Kasting* [1988] noticed a negligible effect for very high cloud opacities since these thick cloud lie too deep to affect radiation, the vertical extent of our cloud layers ensures they always lie at altitudes able to radiate through space, so a direct comparison between both studies is meaningless. Therefore, in the thick limit, nonconservative scattering by the upper clouds becomes the limiting factor significantly reducing thermal leakage from deeper layers. The magnitude of this effect is shown here to depend highly on the optical properties of the cloud particles.

[48] The spectra shown in Figure 8 confirm our interpretation: within absorption bands (such as CO_2 band near 700 cm^{-1} or H_2O past 1200 cm^{-1}), both cloudless and cloudy atmospheres only probe the similar, colder mesospheres, whereas out of this bands, clouds reduce the range of brightness temperatures (and thus layers probed) from a 50 K in the cloudless case down to 30 K for thick Earth-like clouds. As a consequence, the aforementioned KI limit of 160 Wm^{-2} is probably a low estimate, and we only are able to constrain this limit between 160 Wm^{-2} and 200 Wm^{-2} . This range remains nevertheless much lower than previously thought.

3.2.3. Present-Day Venus

[49] In order to further test our model, we can try to reproduce an atmosphere similar to the present-day

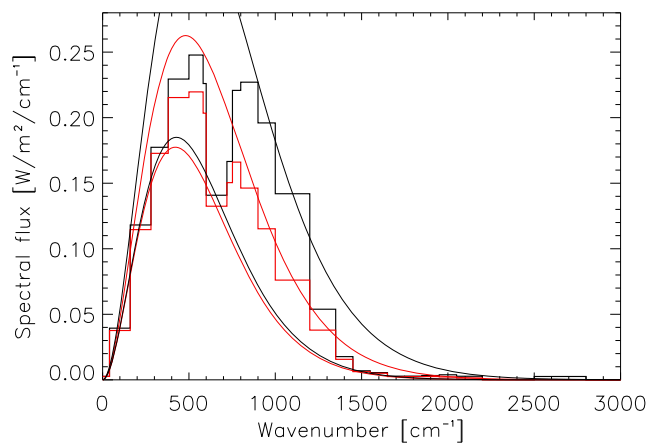


Figure 8. Spectra of thermal radiation with thick water clouds (red lines) and no cloud cover (black lines). Black lines stand for Planck functions at 218 and 270 K, whereas red lines stand for 215 and 245 K. The optical depth of the cloud layer near $1 \mu\text{m}$ is about 100.

atmosphere of Venus. We prescribe $P_n = 9,2 \text{ MPa}$ and $P_v = 300 \text{ Pa}$, since the relative volume mixing for water vapor in the lower atmosphere is close to 3×10^{-5} [*Bailey*, 2009; *Bézar* *et al.*, 2009]. We then adjust T_s so that the effective temperature be equal to the present-day equilibrium temperature of Venus, namely 235 K. It was achieved for a surface temperature $T_s = 745 \text{ K}$, 10 K higher than the measured value [*Pollack et al.*, 1980]. No condensation of water occurs in the equilibrium $T(z)$ profile, and the dry troposphere-mesosphere transition occurs near 61 km, very close to the actual tropopause altitude of Venus near the cloud tops between 65 and 70 km. The nightside spectrum shown in Figure 9 also bears strong similarities with the measured spectrum of Venus [*Allen*, 1987], exhibiting, for example, IR windows of CO_2 near 1.7 and $2.3 \mu\text{m}$, although with an underestimated brightness temperature. Since no cloud layer is formed in our model, and no IR absorption by other species nor the 3.5% of N_2 are taken into account, such an agreement with some qualitative observable properties of the Venesian atmosphere

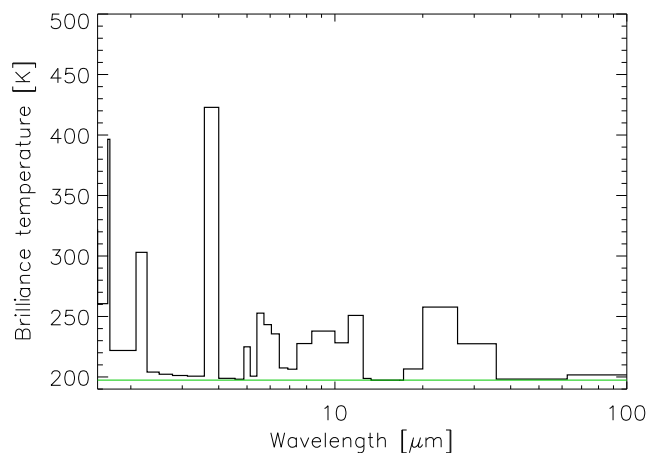


Figure 9. Brightness temperature of the thermal emission of a Venus-like atmosphere.

shows both that our model gives satisfying first-order description of a variety of planetary atmospheres.

4. Discussion

4.1. Shortcomings

[50] Despite the aforementioned results, we would like to warn the reader against the unavoidable shortcomings of such a simple model like ours.

4.1.1. General Concerns

[51] It has been noted that for very high surface temperature and comparatively thin atmospheres, pressure at the tropopause level may be too small to consider local thermodynamical equilibrium (LTE) satisfied. Testing showed that this was not much of a concern for the dense atmospheres studied here ($P \sim 3$ mbar at tropopause for $T_s = 2800$ K, $P_v = 300$ bars and $P_n = 100$ bars).

[52] Also, the thick atmospheres found by our model challenges the plan-parallel approximation. In the worst case, surface area at a height of 600 km is about 20% larger than at ground level, thus impacting significantly the radiative budget. Nevertheless, most radiative exchange in the longwave domain occurs between layers vertically close enough so that plane-parallel approximation remains valid. Also, in most cases, $\tau_{LW} = 1$ is reached at an altitude lower than 300 km, thus reducing the error at about 10%, somewhat less than other uncertainties related to other concerns detailed below.

4.1.2. Clouds

[53] Cloud microphysics is very simplistic, assuming 5 μm water droplets or 1 μm sulphuric acid droplets distributed uniformly in the moist convective layer. Considering the various minor components possibly present in the atmosphere (hydrophilic minor gases such as chlorinated species, possible silicate condensation nuclei), the actual cloud layers were probably very different in terms of optical depth, composition and droplet size distribution from present-day Earth or Venus clouds. Furthermore, near the top of the moist convective layers, temperatures can drop below the freezing point of water, and thus we may expect water ice clouds instead of liquid water droplets. However, we proceeded to what appeared to us as the most sensible assumptions in lack of precise microphysical and chemical models.

4.1.3. Short Wavelengths

[54] A minor shortcoming lies in the approximate radiative equilibrium in the modeled mesospheres. Once solar radiation can be taken into account, it will be possible to calculate a more realistic radiative temperature profile by adjusting $T(z)$ so that the divergence of the net shortwave and longwave fluxes is nullified in the whole mesosphere. For the moment, our temperature adjustment only ensures that the divergence of the thermal radiative flux at the top of our model ($\tau = 0$) is null.

[55] A more serious problem can arise in a situation where a hot surface ($T_s > 2000$ K) coexists with a relatively thin atmosphere. In such a situation, IR windows can probe deep enough in the atmosphere, in layers hot enough so that significant radiation leakage occurs shortward of 1 μm , our current lower bound on wavelengths for the thermal IR calculations. Extending our thermal IR calculations down to, for example, 0.5 μm would be difficult for the following reasons.

[56] 1. CO_2 - CO_2 continuum absorption data are lacking at such lower wavelengths since they have been measured for

Venus at longer wavelengths. Venus is not hot enough to radiate strongly shortward of 1 μm , and scattering (both Rayleigh and aerosol scattering in the clouds) prevents any useful measurement.

[57] 2. The H_2O - H_2O continuum from MT-CKD is available at these wavelengths but not for temperatures higher than 800 K.

[58] Nevertheless, we think it should not have serious consequences for thick enough, water-rich realistic atmospheres for the following reasons: (1) There are numerous water vapor absorption lines in the near IR [Kasting, 1988, Appendix B], so that radiation should come from colder layers for most wavelengths. (2) Rayleigh scattering should add significant opacity at shorter wavelengths, increasing the mean optical path and consequently increasing the probability of absorption. (3) Although CIA is expected to decrease with decreasing wavelength and increasing temperature, such a decrease will be gradual. Even assuming a continuum opacity 1000 times lower in average compared to the value at 1 μm , it merely implies that layers a few scale heights downward are probed, which results in an increase of temperature brightness up to a few hundreds of Kelvins at most. Assuming a uniform IR window with a temperature brightness equal to 1000 K shortward of 1 μm , a very conservative estimate since it neglects any water line absorption or scattering, we find that our model would fail to take into account about 400 Wm^{-2} . We can compare this figure with the 450 Wm^{-2} emitted longward of 1 μm in the atmosphere shown in Figure 2.

[59] To summarize our warnings, underestimation of the thermal IR flux may arise in very specific situations, with the worst possible case being a very hot surface ($T_s > 2000$ K) with no atmosphere at all. For more realistic situations encountered in our modeling, the error should be much less than a factor of 2. More precise upper limits about this underestimation will be computed as the model is being updated and corrected, taking into account even shorter wavelengths in the thermal IR computations despite the lack of observational data. Note that for most of the evolutionary history of the magma ocean atmosphere, we have $T < T_c$, and in such a case, T_B is not expected to exceed 500 K because of cloud scattering, so that no significant underestimation occurs.

4.2. Conclusion and Summary

[60] The 1-D H_2O - CO_2 radiative-convective atmospheric model presented here above, despite the shortcomings (see section 4.1) inherent to its simplicity, has been successful in providing some interesting insights on the early history of telluric atmospheres during the ocean magma stage. More specifically, it points out two separate regimes depending on a comparison between surface temperature and total volatile (H_2O and CO_2) surface pressure.

[61] 1. In the case of a relatively cool surface, the blanketing effect of the atmosphere is strong, resulting in moderate effective temperatures and probable presence of thick water clouds. The thermal spectrum of such atmospheres would be hard to distinguish from more evolved atmospheres comparable to Venus' or even present-day Earth at longer wavelengths. Thermal flux in this situation remains constant at the Komabayashi-Ingersoll limit, estimated between 160 and 200 Wm^{-2} . This range is somewhat lower compared

with previous studies, and is explained by a better treatment of H₂O and CO₂ IR opacities.

[62] 2. In the case of a relatively hot surface, the blanketing effect is overwhelmed and significant thermal cooling can occur in a hot CO₂-steam atmosphere where no condensation takes place. Geologically rapid cooling of the magma ocean is expected in such a situation. Observational characterization of such atmospheres would be comparatively easier because of their overall high brightness temperature in the thermal IR range.

[63] Finally, although this model is intended to be used in complex, integrated magma ocean-atmosphere-escape models, we have thought that separate publication was justified in two ways. First, because of the intrinsic scientific interest of the preliminary results, at least from a qualitative point of view. Second, in order to make this model publicly available for eventual integration into other coupled models subsequently to the coupling to the original coupled model it has been designed for in the first place.

[64] **Acknowledgments.** The author wishes to thank Bruno Bézard, Robin Wordsworth, and Vincent Eymet for their help in the use of KSPECTRUM and insightful discussions. The author also wants to thank Éric Chassefière for initiating the magma ocean coupled model project that this atmospheric model is a part of. Finally, the author is highly grateful to James Kasting and to an anonymous referee for the suggestions they made that improved the quality of this article.

References

- Abe, Y. (1997), Thermal and chemical evolution of the terrestrial magma ocean, *Phys. Earth Planet. Inter.*, *100*(1–4), 27–39, doi:10.1016/S0031-9201(96)03229-3.
- Abe, Y., and T. Matsui (1988), Evolution of an impact-generated H₂O-CO₂ atmosphere and formation of a hot proto-ocean on Earth, *J. Atmos. Sci.*, *45*, 3081–3101, doi:10.1175/1520-0469(1988)045<3081:EOAIGH>2.0.CO;2.
- Allen, D. A. (1987), The dark side of Venus, *Icarus*, *69*, 221–229, doi:10.1016/0019-1035(87)90101-1.
- Bailey, J. (2009), A comparison of water vapor line parameters for modeling the Venus deep atmosphere, *Icarus*, *201*, 444–453, doi:10.1016/j.icarus.2009.01.013.
- Bézard, B., C. de Bergh, D. Crisp, and J.-P. Maillard (1990), The deep atmosphere of Venus revealed by high-resolution nightside spectra, *Nature*, *345*, 508–511, doi:10.1038/345508a0.
- Bézard, B., C. C. C. Tsang, R. W. Carlson, G. Piccioni, E. Marcq, and P. Drossart (2009), Water vapor abundance near the surface of Venus from Venus Express/VIRTIS observations, *J. Geophys. Res.*, *114*, E00B39, doi:10.1029/2008JE003251.
- Clough, S. A., M. W. Shephard, E. J. Mlawer, J. S. Delamere, M. J. Iacono, K. Cady-Pereira, S. Boukabara, and P. D. Brown (2005), Atmospheric radiative transfer modeling: A summary of the AER codes, *J. Quant. Spectrosc. Radiat. Transfer*, *91*, 233–244, doi:10.1016/j.jqsrt.2004.05.058.
- Elkins-Tanton, L. T. (2008), Linked magma ocean solidification and atmospheric growth for Earth and Mars, *Earth Planet. Sci. Lett.*, *271*, 181–191, doi:10.1016/j.epsl.2008.03.062.
- Haar, L., J. Gallagher, G. Kell, and National Standard Reference Data System (U.S.) (1984), *NBS/NRC Steam Tables: Thermodynamic and Transport Properties and Computer Programs for Vapor and Liquid States of Water in SI Units*, Hemisphere, Washington, D. C.
- Hashimoto, G. L., Y. Abe, and S. Sugita (2007), The chemical composition of the early terrestrial atmosphere: Formation of a reducing atmosphere from CI-like material, *J. Geophys. Res.*, *112*, E05010, doi:10.1029/2006JE002844.
- Ingersoll, A. P. (1969), The runaway greenhouse: A history of water on Venus, *J. Atmos. Sci.*, *26*, 1191–1198, doi:10.1175/1520-0469(1969)026<1191:TRGAHO>2.0.CO;2.
- Kasting, J. F. (1988), Runaway and moist greenhouse atmospheres and the evolution of Earth and Venus, *Icarus*, *74*, 472–494, doi:10.1016/0019-1035(88)90116-9.
- Komabayashi, M. (1967), Discrete equilibrium temperatures of a hypothetical planet with the atmosphere and the hydrosphere of one component-two phase system under constant solar radiation, *J. Meteorol. Soc. Jpn.*, *45*, 137–139.
- Meadows, V. S., and D. Crisp (1996), Ground-based near-infrared observations of the Venus nightside: The thermal structure and water abundance near the surface, *J. Geophys. Res.*, *101*, 4595–4622, doi:10.1029/95JE03567.
- Nakajima, S., Y.-Y. Hayashi, and Y. Abe (1992), A study on the “runaway greenhouse effect” with a one-dimensional radiative-convective equilibrium model, *J. Atmos. Sci.*, *49*, 2256–2266, doi:10.1175/1520-0469(1992)049<2256:ASOTGE>2.0.CO;2.
- Pollack, J. B., O. B. Toon, and R. Boese (1980), Greenhouse models of Venus’ high surface temperature, as constrained by Pioneer Venus measurements, *J. Geophys. Res.*, *85*, 8223–8231, doi:10.1029/JA085iA13p08223.
- Schaefer, L., and B. Fegley (2010), Chemistry of atmospheres formed during accretion of the Earth and other terrestrial planets, *Icarus*, *208*, 438–448, doi:10.1016/j.icarus.2010.01.026.
- Stamnes, K., S.-C. Tsay, K. Jayaweera, and W. Wiscombe (1988), Numerically stable algorithm for discrete-ordinate-method radiative transfer in multiple scattering and emitting layered media, *Appl. Opt.*, *27*, 2502–2509, doi:10.1364/AO.27.002502.
- Taylor, F. (2006), Comparative planetary climatology, *Surv. Geophys.*, *27*, 149–167, doi:10.1007/s10712-005-3874-9.
- Wordsworth, R. D., F. Forget, F. Selsis, J.-B. Madeleine, E. Millour, and V. Eymet (2010), Is Gliese 581d habitable? Some constraints from radiative-convective climate modeling, *Astron. Astrophys.*, *522*, A22, doi:10.1051/0004-6361/201015053.
- Wordsworth, R., F. Forget, E. Millour, J.-B. Madeleine, R. M. Haberle, and V. Eymet (2011), Modelling past Mars climates and water cycle with a thicker CO₂ atmosphere, paper presented at 4th International Workshop on the Mars Atmosphere: Modelling and Observation, Cent. Natl. d’Etud. Spat., Paris, 8–11 Feb.
- Zahnle, K. J., J. F. Kasting, and J. B. Pollack (1988), Evolution of a steam atmosphere during Earth’s accretion, *Icarus*, *74*, 62–97, doi:10.1016/0019-1035(88)90031-0.

E. Marcq, LATMOS, Université de Versailles Saint-Quentin-en-Yvelines, 11 Blvd. d’Alembert, F-78280 Guyancourt, France. (emmanuel.marcq@latmos.ipsl.fr)